Inferences about QBO Dynamics from the Atmospheric "Tape Recorder" Effect

TIMOTHY J. DUNKERTON

Northwest Research Associates, Bellevue, Washington

(Manuscript received 16 April 1998, in final form 6 November 1998)

ABSTRACT

Observations of ascending water vapor anomalies in the tropical lower stratosphere—the so-called tape recorder effect—have been used to infer profiles of vertical mean motion, vertical constituent diffusivity, and lateral inmixing rate in this region. The magnitude of vertical wave flux required to drive the quasi-biennial oscillation (QBO) in the presence of mean upwelling, along with other related aspects of QBO dynamics, is examined in light of the tape recorder results using a simple one-dimensional model. As found in a previous study, it is necessary that wave fluxes significantly exceed the ''classic'' values associated with long-period Kelvin and Rossby-gravity waves; the extra fluxes are presumably associated with a continuous spectrum of short-period gravity and inertia–gravity waves. Larger wave fluxes, when used in connection with traditional wave-transport parameterizations developed for the QBO, require a larger vertical diffusivity of momentum in order to prevent the formation of unrealistically strong vertical wind shear. The profile of constituent diffusivity derived from the tape recorder effect, however, is much smaller everywhere than the momentum diffusivity assumed in previous QBO modeling studies.

Realistic shear is obtained in the model using a momentum-conserving ''shear adjustment'' scheme representing the effect of unresolved shear instabilities and other processes not included in the wave-transport parameterization. This device, together with a QBO amplitude profile based on the equatorial-wave phase speeds, motivates an (otherwise inviscid) analytic QBO solution in the underdamped, quasi-compressible case. The simple analytic solutions replicate most aspects of the numerical solution, display a similar dependence on wave flux at the lower boundary, and provide reasonably accurate estimates of QBO period in the inviscid limit.

1. Introduction

The quasi-biennial oscillation (QBO) of the equatorial lower stratosphere was successfully explained 30 years ago by Lindzen and Holton (1968) as being due to the transport of momentum associated with vertically propagating waves. The characteristic feature of the QBO—alternating descent of easterly and westerly shear zones—is implied by a spectrum of upward-propagating easterly and westerly waves, whether the shears form spontaneously (Holton and Lindzen 1972; Plumb 1977) or are initially present aloft (Lindzen and Holton 1968). Lindzen and Holton assumed that a continuous spectrum of gravity waves was responsible for the QBO, while most theoretical studies since then have emphasized the role of a discrete spectrum of equatorial Kelvin and Rossby-gravity waves; the basic mechanism applies in either case. Each wave or spectral component is absorbed approaching its critical level, causing the flow to accelerate in the direction of the shear, so that shear zones descend. Crucial to the theory is a small but nonzero vertical diffusion of momentum near the tropopause, causing the lower jet to decay, so that waves responsible for the lower jet are free once again to propagate to higher levels and an oscillation ensues. This mechanism was demonstrated in the laboratory by Plumb and McEwan (1978).

In the atmosphere, descent of QBO shear zones is opposed by upwelling due to the Brewer–Dobson circulation (Dunkerton 1991). The upwelling is modulated by the QBO, so that easterly shears are slowed to a greater degree (Lindzen and Holton 1968; Holton and Lindzen 1972; Plumb and Bell 1982). Westerly shears are displaced downward at the equator by the QBO circulation anomaly (Hamilton 1984; Dunkerton and Delisi 1985; Dunkerton 1991). A realistic simulation of the QBO depends critically on whether the upward transport and deposition of easterly momentum is sufficient to overcome the tendency for easterly shear zones to be advected upward by the combination of Brewer–Dobson and QBO mean meridional circulations. This problem is further aggravated by a likely westerly bias in the source spectra of equatorial and gravity waves (Dunkerton 1997). Perhaps it is not surprising, then, that the observed QBO has a tendency to stall near 50 mb in the descending easterly phase (Naujokat 1986; Dunkerton 1990).

In order to model the QBO it is necessary to know the rate of upwelling, at least approximately. Obser-

Corresponding author address: Dr. Timothy J. Dunkerton, Northwest Research Associates, P.O. Box 3027, Bellevue, WA 98009.
E-mail: tim@nwra.com

vations of ascending water vapor anomalies in the equatorial lower stratosphere—the so-called tape recorder effect (Mote et al. 1996)—were used by Dunkerton (1997, hereafter D97) to obtain a coarse vertical profile of upwelling on the assumption that the observed rate of anomaly ascent equals the upwelling rate. By calibrating a two-dimensional model to reproduce this upwelling in a control experiment without QBO, and then adding the continuous spectrum of Lindzen and Holton (1968) to a discrete spectrum of equatorial waves, D97 estimated the amount of additional ''gravity wave'' flux required to generate a realistic QBO while holding the fluxes of Kelvin and Rossby-gravity waves close to their observed values. Acceptable values of gravity wave flux at the tropopause, integrated in absolute value over positive and negative phase speeds, were 8–30 $\times$ 10^{-3} m^2 s^{-2}, depending on the experimental configuration (e.g., radiative heating scheme) with values of 15–25 $\times$ 10^{-3} m^2 s^{-2} typically required. The total flux required for a QBO is evidently ~2–4 times as large as that associated with the observed large-scale, long-period Kelvin and Rossby-gravity waves. This inference is consistent with observations of Bergman and Salby (1994), Maruyama (1994), Sato and Dunkerton (1997), and others.

Recently Mote et al. (1998) developed a more sophisticated technique to derive near-equatorial profiles of vertical velocity $\overline{w}_{tr}$, lateral in-mixing rate α, and vertical constituent diffusivity K_{zz} from the tape recorder signal. Observations of ascending total hydrogen anomalies and time-mean methane were used to obtain these parameters at each level by substituting the observed constituent concentrations into an equation containing vertical advection, vertical diffusion, and damping terms representing in-mixing and photochemistry. Three such equations were solved simultaneously (two for the oscillating tape recorder signal, and one for time-mean methane), giving a unique and mostly well-conditioned solution for the three parameters $\overline{w}_{tr}$, α, and K_{zz}. Results of Mote et al. are reproduced in Fig. 1, together with τ, the in-mixing time or inverse of α. The following conclusions may be drawn from their work.

a. Vertical velocity

The profile of $\overline{w}_{tr}$ is similar to the diabatic vertical velocity of Rosenlof (1995) derived from a sophisticated radiative code and lies within the range of values inferred previously by Dunkerton (0.25–0.60 mm s^{-1}) though tending toward the lower end of this range (0.20–0.40 mm s^{-1}). The altitude of minimum upwelling near 20 km agrees better with Rosenlof's profile. The small discrepancy between diabatic and ''observed'' vertical velocity below this altitude may be due to vertical constituent diffusivity, the observed values in the tape recorder signal corresponding approximately to

$$\tilde{w} = \overline{w} + \frac{K_{zz}}{H} - \frac{\partial K_{zz}}{\partial z}, \qquad (1.1)$$

where H is the density-scale height (D97; Mote et al. 1998). In a shallow layer above the tropopause, a rapid decrease of K_{zz} with altitude will enhance the rate of anomaly ascent over the actual rate of upwelling. One may refer from the ''new and improved'' profile of $\overline{w}_{tr}$ that values of wave flux required for a realistic QBO remain close to (or perhaps slightly smaller than) those obtained by D97.

b. Lateral mixing

The profile of α, largely determined by the methane balance, decreases rapidly to a minimum around 21–22 km, corresponding to a damping time of about 80 months, and increases more slowly above this altitude. The minimum in-mixing rate is notably smaller than inferred in other studies (e.g., Hall and Waugh 1997; Schoeberl et al. 1997) wherein bulk estimates were made. But if such a timescale is also relevant to the dynamical QBO, the calculated α minimum is reasonable since the observed westerly regimes near 20 km are unusually persistent, lasting 12–18 months without attenuation (until the next easterly onset). The long duration of westerlies in the lower QBO region coincides with an absence of planetary wave breaking noted by O'Sullivan (1997) in simulations with a barotropic model and by O'Sullivan and Dunkerton (1997) in observations of long-lived trace constituents. Larger values of α above and below 20–24 km imply that lateral mixing could play a role in the QBO dynamics, where τ falls below the period of the QBO (~22–36 months). Planetary Rossby waves are involved in the onset of easterlies in the upper QBO region (Ortland 1997), while synoptic-scale eddies and monsoon circulations are important for lateral mixing just above the tropopause (Trepte and Hitchman 1992; Trepte et al. 1993; Hitchman et al. 1994; Chen 1995; Dunkerton 1995).

c. Vertical diffusion

Mote et al. (1998) obtained robust estimates of K_{zz} in the 19–24-km layer, but there is considerable uncertainty above and below. Their ''best'' estimate, with tape recorder attenuation rate constrained to a constant above ~26 km, implies positive K_{zz} in this region (diamonds). Unfortunately, most estimates of K_{zz} were ill-conditioned near the tropopause (not shown). A shallow ''skirt'' of increasing K_{zz} toward the tropopause could be inferred indirectly from the discrepancy between diabatic and observed vertical velocity in this region, as noted above, indicated by a dashed line and ''?'' symbol. Values of vertical constituent diffusivity K_{zz} derived by Mote et al. are everywhere much smaller than the values of vertical momentum diffusivity used in previous QBO modeling studies (e.g., Holton and Lindzen 1972; D97) on the order of 0.3 m^2 s^{-1} or more. The bulk estimate of $K_{zz} \approx 0.01$ m^2 s^{-1} derived by Hall and Waugh (1997) is also very small. Additional calculations by the author

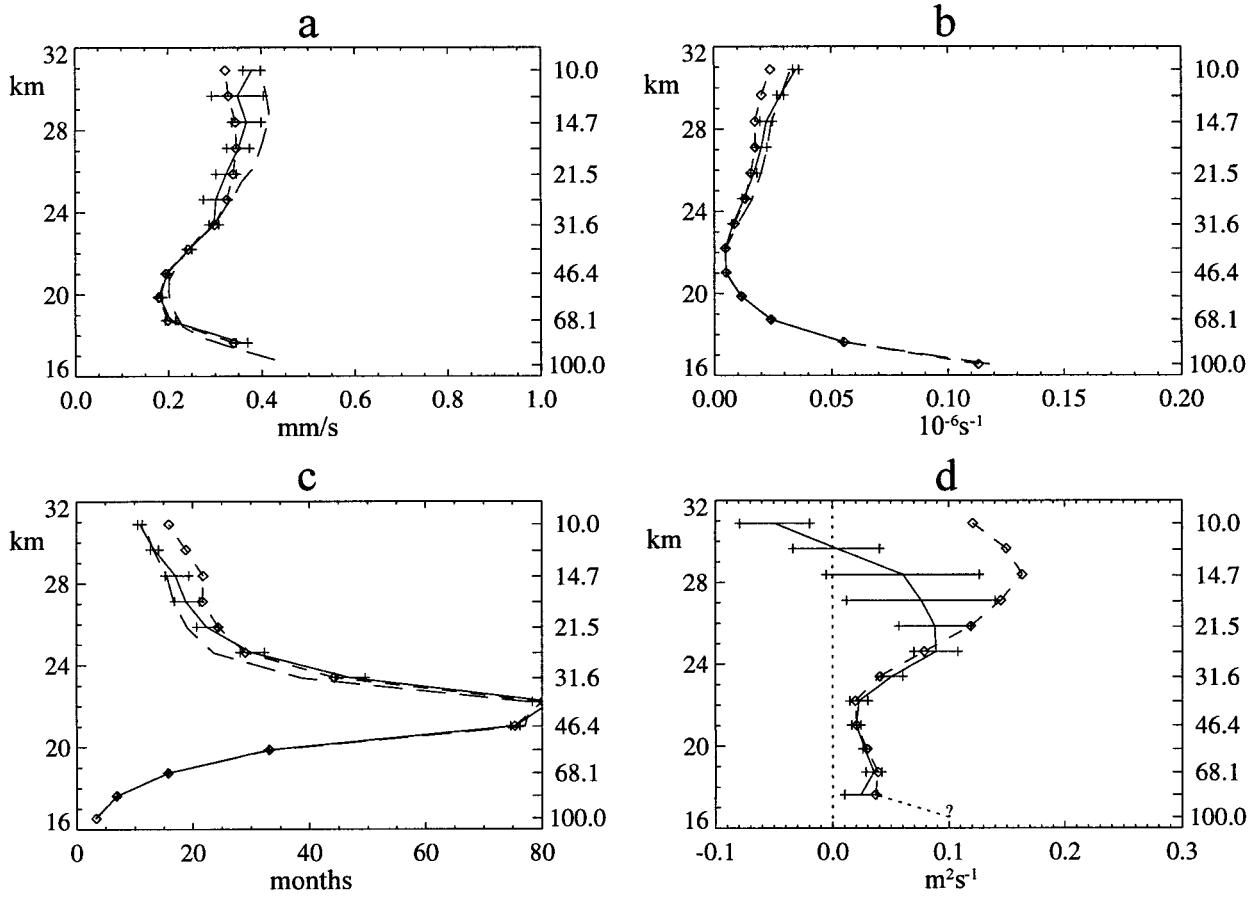

FIG. 1. Profiles of (a) vertical velocity $\overline{w}_{tr}$, (b) lateral in-mixing rate α, (c) in-mixing time τ, and (d) vertical constituent diffusivity K_{zz} derived from the tape recorder signal. The range of values obtained with different approximations to tape recorder amplitude is indicated by horizontal bars; diamonds show the special case with constant attenuation rate above ~26 km. (d) The indirect estimate of K_{zz} approaching the tropopause is shown by a dotted line and "?" symbol. Adapted from Mote et al. (1998).

using the one-dimensional model of Mote et al. suggest that an increase of K_{zz} would either cause excessive attenuation of the tape recorder signal or would substantially overestimate the vertical wavelength of this signal.

While a QBO may be theoretically possible for any small but nonzero K_{zz} (Plumb 1977), a practical difficulty is that vertical shears are excessively strong (above the tropopause and throughout the stratosphere) without adequate vertical diffusion of momentum. This problem is further aggravated by larger values of wave flux required to overcome Brewer–Dobson upwelling. A rough estimate of the required momentum diffusivity can be obtained from the steady-state balance when a QBO regime takes hold above the tropopause:

$$\overline{v}^*\left(\frac{\partial \overline{u}}{\partial y} - f\right) + \overline{w}^*\frac{\partial \overline{u}}{\partial z} = \frac{1}{\rho_0}\frac{\partial}{\partial z}\rho_0 \nu \frac{\partial \overline{u}}{\partial z} - \frac{1}{\rho_0}\nabla \cdot \mathbf{F}, \quad (1.2)$$

where $\overline{v}^*$ and $\overline{w}^*$ are meridional and vertical mean velocity (transformed Eulerian mean), f is the Coriolis parameter, $\rho_0 = \rho_s \exp(-z/H)$ is basic-state density, ν is the vertical diffusivity of momentum, and $\mathbf{F}$ is the Eliassen–Palm flux (Andrews and McIntyre 1976). Neglecting mean advection and effects of lateral propagation or mixing, the balance between vertical diffusive flux and vertical wave flux is

$$\rho_0 \nu \frac{\partial \overline{u}}{\partial z} = F_{(z)}. \quad (1.3)$$

If the observed maximum QBO shears (10–15 m s^{-1} km^{-1}) are to coexist at steady state with vertical wave fluxes of magnitude ~6–21 × 10^{-3} m^2 s^{-2} as inferred by D97, the required vertical diffusivity of momentum evidently must lie in the range 0.4–2.1 m^2 s^{-1}. This is a factor of 4–100 times larger than the values of vertical constituent diffusivity derived by Mote et al. (1998) but consistent with QBO modeling experiments including the effects of mean meridional and vertical advection (D97).

This argument does not depend on the choice of wave-transport parameterization. Schemes traditionally used in QBO models (Lindzen and Holton 1968; Holton

and Lindzen 1972) are to blame for the formation of large or infinite vertical shear. Whether such schemes are entirely realistic is open to debate, but strong shear is undoubtedly a natural consequence of vertical wave propagation in the equatorial atmosphere, whether from discrete (underdamped) waves (Dunkerton 1981a) or a continuous spectrum (Lindzen and Holton 1968). Once formed, a shear zone concentrates the breaking or absorption of a broad spectrum of waves into a shallow layer, tending to strengthen the shear and further concentrating the acceleration. This mechanism has been documented in numerical and laboratory studies (Dunkerton and Fritts 1984; Delisi and Dunkerton 1989) and is expected in more general circumstances. Reflection of waves will return some momentum to the troposphere and may limit the magnitude of shear attainable due to wave–mean flow interaction alone (Plumb 1977). In this event, the incident flux would have to be increased to compensate for reflection unless the reflected flux is absorbed within the shear zone. Refraction of high-frequency waves by low-frequency waves might allow some waves initially to escape absorption (Broutman et al. 1997) but the effect would be temporary: in *mean* vertical shear, there is ultimately no escape for upward-propagating waves with critical levels in the flow.

Instabilities prevent the formation of very large vertical shear in the atmosphere. It is reasonable to assume that the shear cannot exceed some threshold. However, the limiting values of QBO shear observed in monthly mean data imply a local Richardson number on the order of 1–4, well above the threshold of Kelvin–Helmholtz or inertial instability (Stone 1966; Hazel 1972). The large-scale monthly mean flow is not unstable in this sense, but patches of instability and turbulence are expected intermittently in space and time as various kinds of wave motion superpose on themselves and on the mean shear to produce locally unstable regions, as observed in the laboratory (Delisi and Dunkerton 1989). The resulting monthly mean shear is therefore smaller than the local threshold for instability. A statistical treatment of the problem is beyond the scope of this paper and requires further analysis of available rawinsonde data at equatorial stations.

As a practical matter, turbulent mixing is required and is likely to occur primarily in descending shear zones. Such local mixing would affect the vertical distribution of momentum (having a strong vertical gradient) much more than the vertical distribution of tracer (lacking a strong vertical gradient). It may be difficult to detect the influence of shear-zone mixing in tracer fields with relatively coarse vertical resolution. Nevertheless, given the large discrepancy that exists between the coefficient of constituent diffusivity derived from the tape recorder signal and the coefficient of momentum diffusivity required in QBO models, the mixing of momentum is probably more efficient than the mixing of constituents, as implied by earlier theoretical studies, which suggests a large ''turbulent Prandtl number'' in breaking gravity waves (Fritts and Dunkerton 1985; Coy and Fritts 1987).

The data do not permit a temporally varying K_{zz} to be derived from the tape recorder signal; application of a constituent diffusivity to momentum, in any case, would be uncertain owing to the Prandtl number question. The purpose of this paper is to discuss a simpler model of the QBO in which the explicit, time-independent vertical momentum diffusivity is eliminated and is replaced by a local mixing process known as ''shear adjustment,'' equivalent to mixing of the horizontal component of vorticity within descending shear zones, designed to conserve vertically integrated momentum but to prevent formation of unrealistic shear. In the otherwise inviscid limit (with specified momentum diffusivity equal to zero) shear adjustment is the only mechanism controlling the strength of the shear. This device leads to a simpler description of the evolution of the QBO: namely, shear zones of prescribed strength descend within a QBO ''amplitude envelope'' until encountering a ''boundary layer'' above the tropopause. In general, the amplitude envelope, shear-zone strength, and boundary layer depth are part of the QBO solution, but motivated by some simple numerical experiments discussed in section 2, it will be assumed that these variables are known. The situation just described can be solved analytically for various kinds of source spectra, affording a comparison to the numerical results and providing new insights into the dynamics of the QBO.

2. One-dimensional model

The one-dimensional model of Holton and Lindzen (1972) was generalized by D97 to include a continuous spectrum of gravity waves (Lindzen and Holton 1968) and a linear regression for vertical velocity as a function of equatorial vertical shear $\partial\overline{u}/\partial z$. This approach reproduced the results of a two-dimensional model with minor differences. For example, a semiannual oscillation in the upper stratosphere (not included in the 1D model) tends to synchronize the onset of new QBO regimes (Dunkerton and Delisi 1997). Horizontal advection by the Hadley circulation in the 2D model prevents the QBO from entering the troposphere, reinforcing the effect of vertical advection in this region (Saravanan 1990). The 1D and 2D models otherwise produce similar vertical structures and QBO period. For this study, the 1D model was integrated at fine vertical resolution (150 m) for improved accuracy in cases with reduced diffusion and strong vertical shear.

a. Governing equations

The one-dimensional model solves an equation for mean zonal wind of the form

$$\frac{\partial \overline{u}}{\partial t} + \overline{w}^* \frac{\partial \overline{u}}{\partial z} = \frac{1}{\rho_0} \frac{\partial}{\partial z} \rho_0 \nu \frac{\partial \overline{u}}{\partial z} + \alpha(\overline{u}^E - \overline{u}) + A_{\text{eqw}}(z, t) + A_{\text{gw}}(z, t), \quad (2.1)$$

where A_{eqw} and A_{gw} are the body force per unit mass due to equatorial and gravity waves, respectively, and

$$\nu = \text{Pr} K_{zz}, \quad (2.2)$$

where Pr is an effective turbulent Prandtl number, assumed constant for simplicity. Vertical velocity is determined by linear regression with respect to equatorial vertical shear as

$$\overline{w}^* = a(z) + b(z) \frac{\partial \overline{u}}{\partial z} \quad (2.3)$$

using results from a two-dimensional simulation for the coefficients a, b following D97. In this paper, values of $\overline{w}_{\text{tr}}$ from Mote et al. (1998) were substituted for a in the tape recorder region.

Large-scale equatorial waves were parameterized as before; for each wave, the latitudinally integrated vertical component of Eliassen–Palm flux is determined by an equation of the form

$$B(z) = B(z_0) \exp\left[\frac{(z - z_0)}{H} - P(z)\right] \quad (2.4a)$$

$$P(z) = \int_{z_0}^{z} D(z')\, dz', \quad (2.4b)$$

where $D(z)$ is the dissipation rate (m^{-1}). Steady waves are assumed in (2.4), slowly varying in height, damped by scale-dependent radiative damping using an analytic fit to Fels' (1982) $\alpha_T(m, z)$, as done by D97 and previous authors. The wave-induced mean flow acceleration is of the form

$$A_{\text{eqw}} = \hat{a}(\xi) D(z) B(z_0) \frac{\exp[(z - z_0)/H - P(z)]}{y_0}, \quad (2.5)$$

where $\hat{a}(\xi)$ is a nondimensional acceleration profile (Andrews and McIntyre 1976), normalized such that $\int_{-\infty}^{\infty} \hat{a}(\xi)\, d\xi = 1$, and $\xi = y/y_0$, that is, dimensional latitude divided by the meridional scale of the wave y_0. Profiles of $\hat{a}(\xi)$ for Kelvin and Rossby-gravity waves were given in Dunkerton (1985). The one-dimensional model solves for equatorial zonal wind only ($\xi = 0$). The quantity $B(z_0)$ is related to the local vertical component of Eliassen–Palm flux $F_{(z)}$ as

$$\rho_s B(z_0) = \int_{-\infty}^{\infty} F_{(z)}\, dy = \frac{F_{(z)}(\xi_{\max}, z_0) y_{00}}{\hat{b}(\xi_{\max})}, \quad (2.6)$$

where $\hat{b}(\xi)$ is a nondimensional profile of $F_{(z)}$, normalized such that $\int_{-\infty}^{\infty} \hat{b}(\xi)\, d\xi = 1$, y_{00} is the meridional scale at z_0, and $\xi_{\max}$ is the nondimensional latitude of maximum $F_{(z)}$. For the Rossby-gravity wave, the effective $\beta_M = [\beta(\beta - \overline{u}_{yy})]^{1/2}$ is determined by linear regression with respect to the equatorial wind using results from a two-dimensional simulation, as in D97. The effect of a continuous gravity wave spectrum is represented by

$$A_{\text{gw}} = |\mathcal{B}_0(\overline{u})| \frac{\partial \overline{u}}{\partial z} \exp\left[\frac{(z - z_0)}{H}\right], \quad (2.7)$$

following Lindzen and Holton (1968). The momentum flux for each spectral element is assumed constant up to a critical level $\overline{u}(z_c) = c$, if one exists, and is set to zero above this level. The gravity wave spectrum was specified as

$$\mathcal{B}_0(c) = \frac{B(z_0)}{2c_1} \frac{|c|}{c_1} \exp - \frac{|c|}{c_1}, \quad (2.8)$$

with $c_1 = 10$ m s^{-1}, as shown in Fig. 3 of D97.

The one-dimensional model described above differs from that of Holton and Lindzen (1972). Mean zonal wind is integrated *at* the equator rather than an average over the equatorial waveguide, as equatorial and gravity waves are assumed to respond primarily to the equatorial wind. Momentum is not perfectly conserved by the governing 1D equations (although it is properly conserved in the 2D model) because 1) equatorial waves contract in latitude approaching their critical level, causing momentum transport to be focused onto the equator from adjacent latitudes; and 2) the mass-weighted vertical velocity depends on altitude.

b. Shear adjustment

Vertical shear must be simulated realistically on account of the regression (2.3) so that QBO temperature and induced circulation anomalies have reasonable amplitude. For this purpose an adjustment routine was added to the numerical code to keep the magnitude of shear within bounds. At each time step, if the shear exceeded a specified maximum amplitude, the vertical profile of $\overline{u}$ was adjusted using a simple procedure. Two limiting profiles of $\overline{u}$ may be defined, each with the maximum allowed shear but differing in their starting altitude. One profile is tangent to the original profile at the base of the region in which the maximum shear is exceeded, and the other is tangent to the wind profile at the top of this region. The final, adjusted profile is a unique linear combination of the two having the same vertically integrated momentum as the original, unadjusted profile. The adjustment was applied separately to easterly and westerly shear, as needed. Observed shears of monthly mean zonal wind in the QBO region are typically 10 m s^{-1} km^{-1} and do not exceed 15 m s^{-1} km^{-1} (Sato and Dunkerton 1997). For simplicity, the limiting value of shear was assumed constant in height, although observations suggest some altitude dependence.

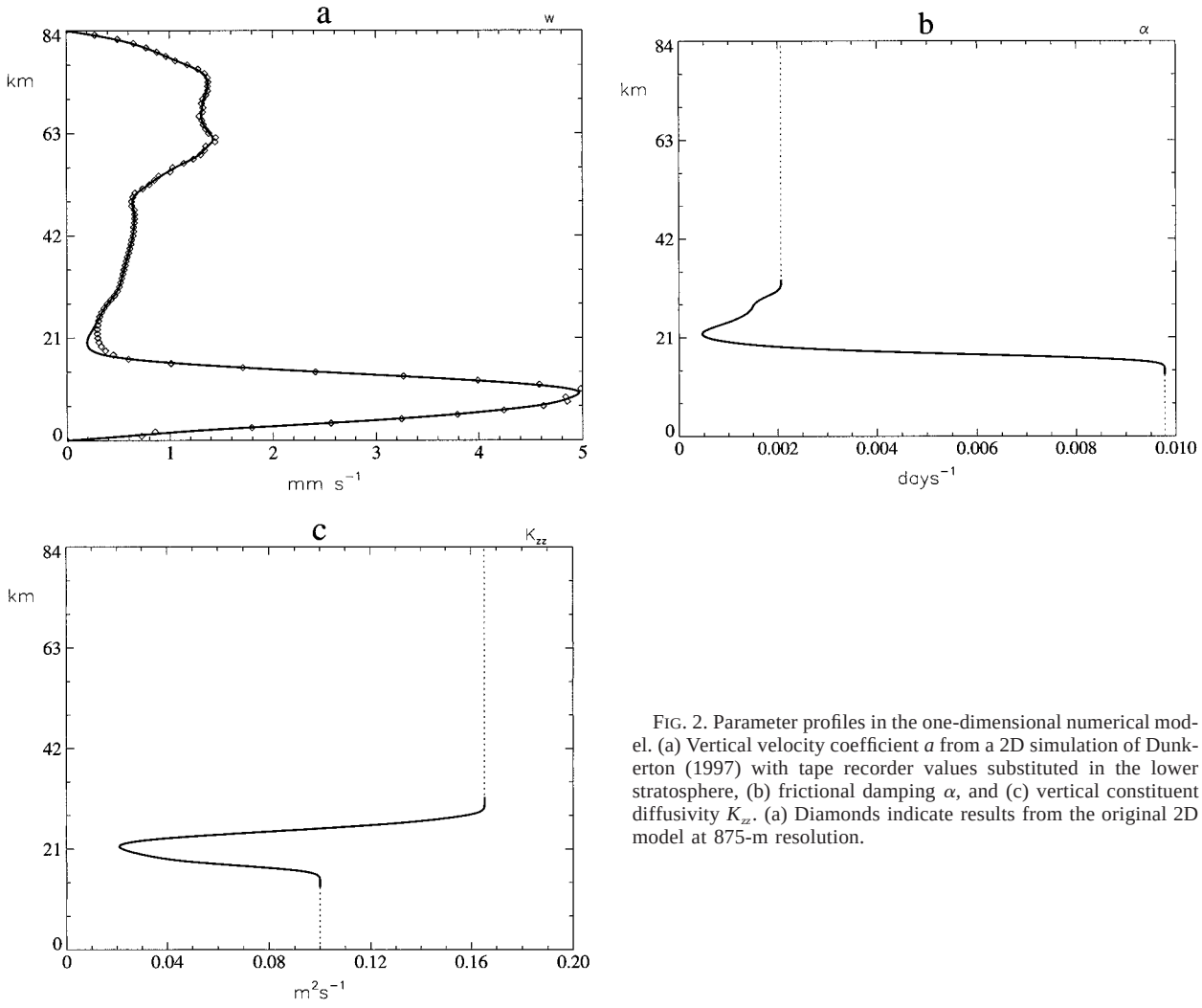

FIG. 2. Parameter profiles in the one-dimensional numerical model. (a) Vertical velocity coefficient a from a 2D simulation of Dunkerton (1997) with tape recorder values substituted in the lower stratosphere, (b) frictional damping α, and (c) vertical constituent diffusivity K_{zz}. (a) Diamonds indicate results from the original 2D model at 875-m resolution.

c. Input parameters

A few parameter profiles for the one-dimensional model are shown in Fig. 2. The regression coefficient $a(z)$ for vertical velocity, shown in Fig. 2a, was obtained from the simple experiment in section 4.2 of D97 (three equatorial waves, with Newtonian relaxation for thermal forcing of the mean state) except that tape recorder values of upwelling from Mote et al. (1998) were substituted for $a(z)$ in the height range ~18–26 km. This substitution reduced the minimum vertical velocity to roughly two-thirds of its original value and lowered the altitude of the minimum by about 1 km. Values of $b(z)$, shown in Fig. 15b of D97, are negative and relatively small in the QBO region, but are important for the QBO dynamics (D97). Regression coefficients for effective β_M in the Rossby-gravity wave routine (not shown) display the enhancement of cross-equatorial curvature in QBO westerlies and vice versa. Frictional damping was added to the code, using the tape recorder profile of α where defined (set to a constant above and below), as shown in Fig. 2b, although its effect proved to be minor. The flow was relaxed to a weak easterly value $\overline{u}^E = -5$ m s^{-1} throughout the domain (easterlies and westerlies alike). The vertical constituent diffusivity, shown in Fig. 2c, was also obtained from Mote et al. (1998) where defined, except that values above and below the midsection (~19–28 km) were replaced by constant values. In the example shown, the profile immediately below 19 km was extended to match the indirect estimate of K_{zz} at the tropopause (0.1 m^2 s^{-1}).

d. Realistic simulation

A simple QBO simulation similar to that described in section 4.2 of D97 was repeated in the one-dimensional model at fine vertical resolution $\Delta z = 150$ m, with time step $\Delta t = 8640$ s, using the input parameter profiles described above. For the first Kelvin wave,

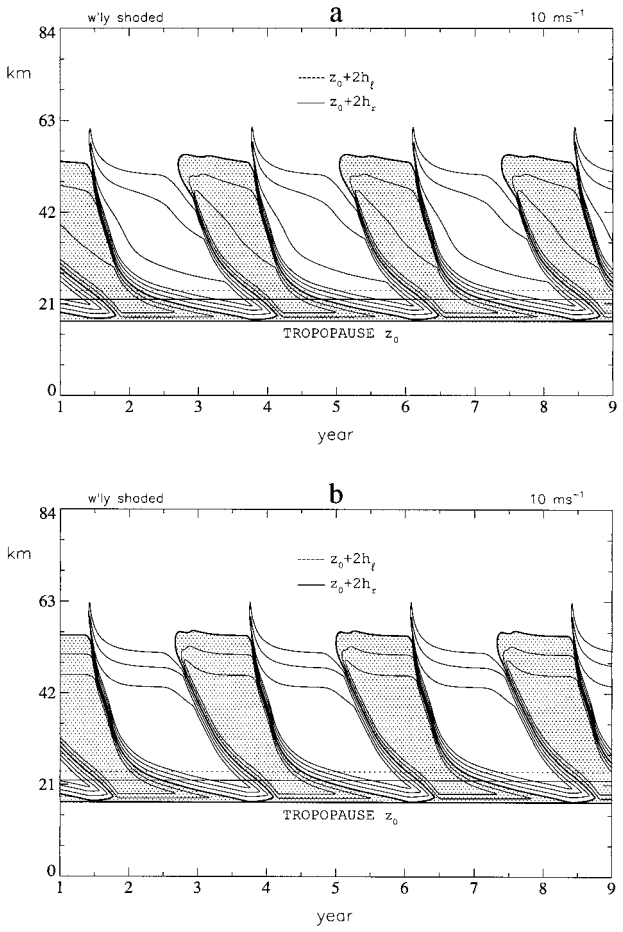

FIG. 3. Mean zonal wind in the one-dimensional numerical model (a) with frictional damping α and (b) without frictional damping. Contour interval is 10 m s^{-1}, and westerlies are shaded. Horizontal lines indicate a distance above the tropopause equal to twice the depth of nominal westerly (solid) and easterly (dotted) boundary layers.

$$k_{\mathrm{KQ}_1}a = 2 \tag{2.9a}$$

$$c_{\mathrm{KQ}_1} = 30 \text{ m s}^{-1} \tag{2.9b}$$

$$B_{\mathrm{KQ}_1}(z_0) = 2.5 \times 10^{-3} \text{ m}^2 \text{ s}^{-2}; \tag{2.9c}$$

for the second Kelvin wave,

$$k_{\mathrm{KQ}_2}a = 2 \tag{2.10a}$$

$$c_{\mathrm{KQ}_2} = 20 \text{ m s}^{-1} \tag{2.10b}$$

$$B_{\mathrm{KQ}_2}(z_0) = 2.5 \times 10^{-3} \text{ m}^2 \text{ s}^{-2}; \tag{2.10c}$$

and for the Rossby-gravity wave,

$$k_{\mathrm{RG}}a = 4 \tag{2.11a}$$

$$c_{\mathrm{RG}} = -40 \text{ m s}^{-1} \tag{2.11b}$$

$$B_{\mathrm{RG}}(z_0) = -2.5 \times 10^{-3} \text{ m}^2 \text{ s}^{-2}, \tag{2.11c}$$

where z_0 is the tropical tropopause height (17 km) and a is the radius of the earth. To prevent QBO regimes from entering the upper troposphere, we set $\overline{u}(z_0) = 0$, following Holton and Lindzen (1972), noting that vertical advection alone is insufficient for this purpose (D97). The gravity wave flux $B_{\mathrm{GW}}(z_0)$ in (2.8) can be regarded as a tunable parameter determining the period of the QBO. Various combinations of $B_{\mathrm{GW}}(z_0)$, Λ (the maximum absolute value of shear), and Pr were examined, as discussed in section 4. For illustration, we consider a particular case,

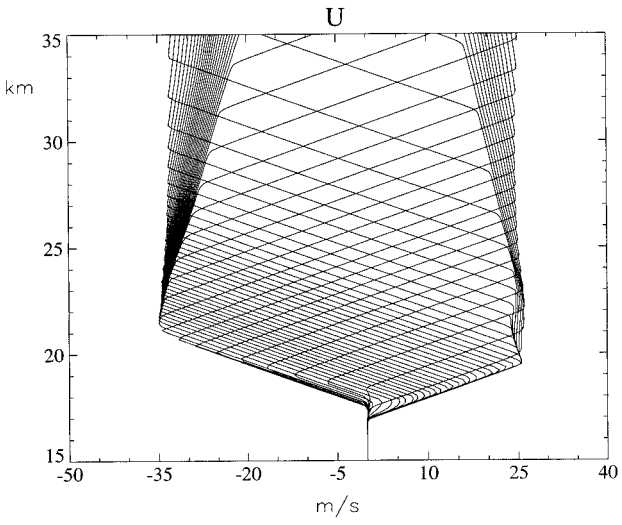

FIG. 4. Profiles of mean zonal wind at 20-day intervals from simulation of Fig. 3a.

$$\mathrm{Pr} = 1 \tag{2.12a}$$

$$\Lambda = 10 \text{ m s}^{-1} \text{ km}^{-1} \tag{2.12b}$$

$$B_{\mathrm{GW}}(z_0) = 22.7 \times 10^{-3} \text{ m}^2 \text{ s}^{-2}, \tag{2.12c}$$

for which the period of the simulated oscillation is 841 days, as shown in Fig. 3a.

The mean zonal wind is realistic in several respects: westerlies are relatively long-lived at lower levels and vice versa; easterlies descend rapidly at first (more rapidly than westerlies) but are retarded by vertical advection at lower levels; and easterlies are stronger than westerlies except near the base of the QBO. The amplitude of QBO is somewhat too strong above the tropopause. The asymmetry of easterly and westerly regimes is due to the combination of asymmetric forcing and vertical advection. Shear zones are realistic by decree, limited to the maximum value specified in (2.12b). The corresponding experiment without tape recorder friction is shown in Fig. 3b, with $B_{\mathrm{GW}}(z_0) = 24.1 \times 10^{-3}$ m^2 s^{-2} and period 838 days. The vertical structure is similar, but QBO regimes maintain constant strength until replaced by the next phase.

Simulated profiles of $\overline{u}$ at each time step are remarkably simple. A complete cycle from Fig. 3a is illustrated in Fig. 4 for the lower part of the QBO (15–35 km). In this altitude range the simulated QBO amplitude is roughly constant above a boundary layer that extends

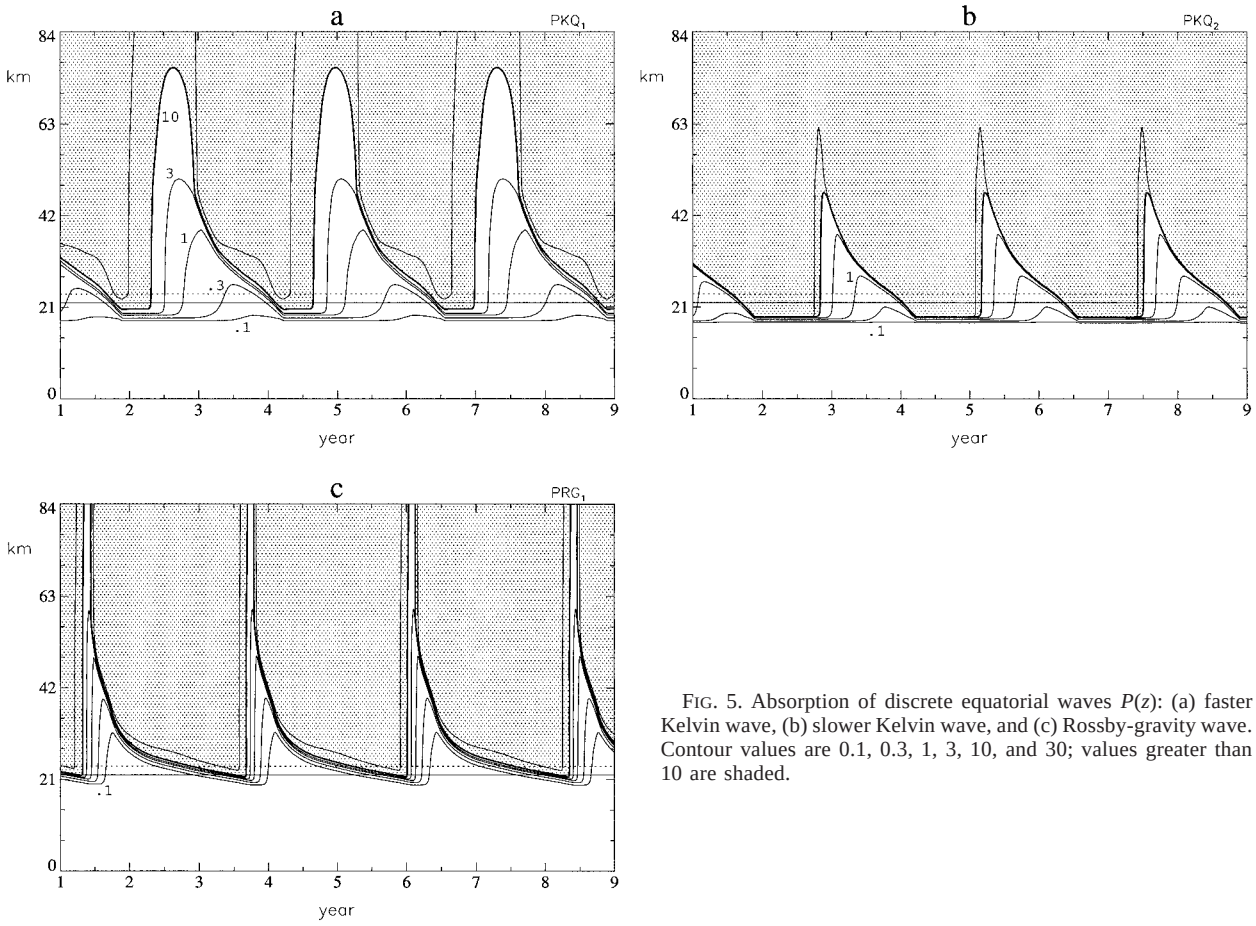

FIG. 5. Absorption of discrete equatorial waves $P(z)$: (a) faster Kelvin wave, (b) slower Kelvin wave, and (c) Rossby-gravity wave. Contour values are 0.1, 0.3, 1, 3, 10, and 30; values greater than 10 are shaded.

to 19.5 km for westerlies and to about 21.5 km for easterlies. The height of the boundary layer is dictated by the imposed maximum shear and maximum QBO amplitude in both phases, but for the easterly phase the boundary layer top is elevated slightly higher because easterly shears do not descend all the way to the tropopause. We refer to this behavior as an *occlusion* reflecting the fact that easterly regimes are permanently cut off from the troposphere.

The descent of westerly shear in Fig. 4 is fairly uniform in time while easterly shears slow down approaching 20 km. In the model stratosphere, decay of QBO regimes due to friction is slow relative to shear-zone descent. The maximum amplitude of the QBO is almost independent of height in this range, and QBO regimes retain most of their original strength prior to descent of the next shear zone. Without tape recorder friction, as shown in Fig. 3b, QBO regimes maintain virtually all of their original strength. This behavior motivates a simple theoretical model of the QBO in which shear zones of constant Λ descend within a fixed ''amplitude envelope'' until encountering the boundary layer. Analytic solutions for this model are discussed in the following section.

The gravity wave spectrum is essential for the simulated oscillation to exist and to have a reasonable period in the presence of Brewer–Dobson upwelling (D97). Discrete equatorial waves are also essential and determine the maximum amplitude of the QBO. In this case, the amplitude is about 85% of the Kelvin and Rossby-gravity phase speeds. Damping of equatorial waves is very sensitive to the prevailing wind, as shown in Fig. 5, illustrating the quantity $P(z)$ (analogous to optical depth). As it turns out, each wave displays a somewhat different absorption pattern. The Rossby-gravity wave (Fig. 5c) is generally ''underdamped'' until encountering the maximum wind at the top of the easterly shear zone, so that momentum flux is approximately conserved and the descending easterly shear feels the maximum strength of this wave. This behavior is similar to that of the conservative gravity wave spectrum, but not necessarily realistic, since our Rossby-gravity parameterization neglects mechanical damping, which would significantly enhance the dissipation rate. The faster Kelvin wave (Fig. 5a) is also underdamped but is somewhat less sensitive to the mean wind than the Rossby-gravity wave. Transmission to upper levels begins earlier, and there is noticeable attenuation of this

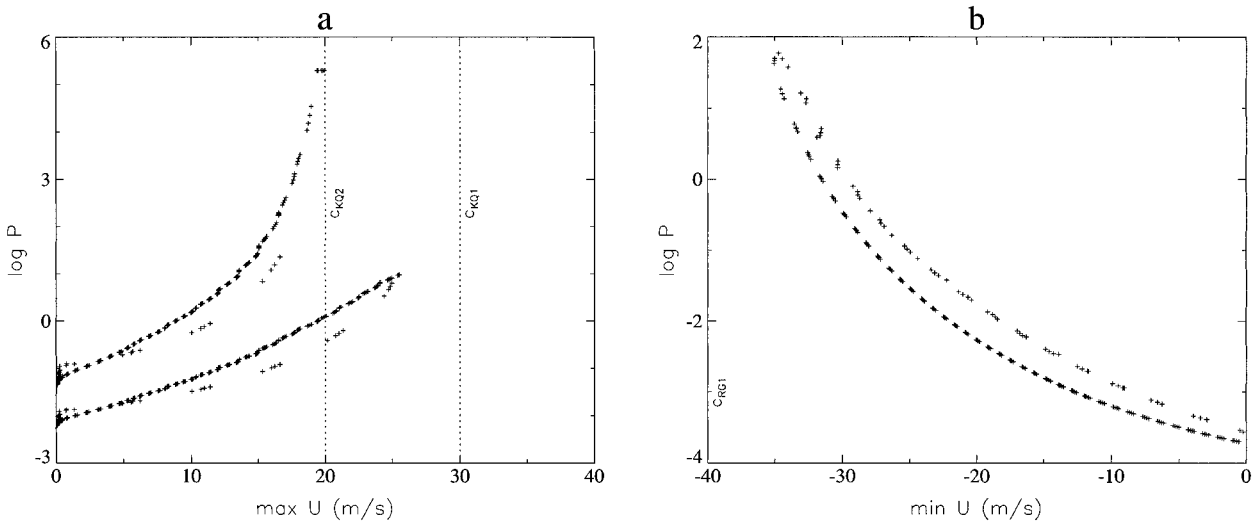

FIG. 6. Values of $P(z)$ at the top of the westerly (easterly) boundary layer plotted with respect to the maximum (minimum) mean zonal wind in the respective boundary layers: (a) fast and slow Kelvin waves and (b) Rossby-gravity wave. Data were sampled at 10-day intervals from a 10-yr simulation.

wave below the descending westerly shear zone. The slower Kelvin wave (Fig. 5b) is the only one of the three to encounter a critical level—a complete barrier to propagation—and the release of this wave is significantly delayed. The attenuation, moreover, is severe. This wave is generally ''overdamped,'' the momentum flux decaying more rapidly with height than ρ_0.

In each case, isopleths of $P(z)$ are approximately vertical in the stratosphere after the waves resume their vertical propagation. Thus, the initial absorption occurs mostly in the boundary layer flow, which determines not only the ''release time'' for each wave but also the transmission of momentum flux once propagation resumes. A compact relationship exists between P at the top of the boundary layer and the maximum boundary layer wind (for westerly waves) or minimum boundary layer wind (for easterly waves) as shown in Figs. 6a–c. The location and shape of each of these curves are consistent with the description above.

An analogy can therefore be made between the transmission of discrete waves and transmission of a continuous gravity wave spectrum: the amount of momentum flux transmitted to higher altitudes is mostly determined by the extrema of boundary layer flow. For otherwise-conservative gravity waves, it is simply a question of how many waves avoid critical-level absorption in the boundary layer. The transmitted flux equals the source spectrum integrated over the range of surviving phase speeds. For each damped equatorial wave, the degree of damping is determined by the proximity of underlying mean flow extremum to the wave's phase speed. Formulas similar to (A13) in the appendix of D97 may be used to approximate the integrated boundary layer damping. The problem is further simplified by constant (limiting) vertical shear as assumed here.

3. Analytic solution

a. Formulation

The behavior of $\overline{u}$ in the nearly inviscid case with shear adjustment can be idealized as shown in Fig. 7. The oscillation has constant amplitude above a boundary layer, the depth of which is determined by the maximum amplitude of each phase and the imposed maximum vertical shear. Evolution of descending shear zones can be described entirely in terms of the position of zero-wind lines $z_{r,i}$ and $z_{\ell,i}$, where the subscripts r and ℓ refer to rightward (westerly) and leftward (easterly) shear zones. The upper and lower limits of each shear zone are determined either 1) as the point of intersection with the QBO envelope, as shown at the upper end of ''A''; or 2) as the average of zero-wind altitudes between adjacent shear zones, when shear zones intersect *inside* the QBO envelope, as shown at the lower end of ''A.'' This simple geometric argument suffices because the maximum absolute value of vertical shear is the same for rightward and leftward shear zones. The rate of shear-zone or zero-wind line descent is determined by the total wave momentum flux imparted to the shear zone, as discussed momentarily, less any upward tendency due to upwelling. In asymmetric cases it is possible for a shear zone to overtake the one immediately below, as shown in ''B.'' There is no longer a zero-wind line for either shear zone, but a pair of virtual zero-wind lines may be used to track the altitude of each. Their intersection point is once again the average of the two virtual zero-wind altitudes, although the older shear zone is now ''above'' the newer one when their position is defined in this way. The older shear zone continues to evolve after being overtaken by the newer one, until the latter intersects the boundary layer, at

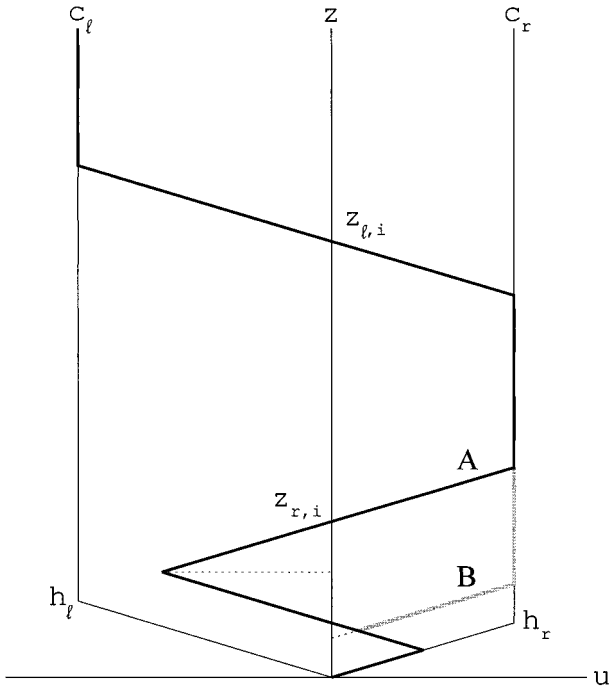

FIG. 7. Idealized QBO for analytic solution. Shear zones of specified strength descend within a fixed amplitude envelope with vertical sidewalls and sloping boundary layers. The height of zero-wind lines z_i, z_{i-1}, etc., is used to denote shear-zone position. The normal situation is labeled ''A,'' while the occluded case is indicated by ''B.''

which point the older shear zone is discarded since it no longer exists.

To calculate the rate of shear-zone descent, we note first of all that the area between an initial shear zone and one displaced downward by a small distance ϵ can be divided into three regions: a parallelogram in the center and a right triangle at each end. The area of the triangles is $O(\epsilon^2)$ and may be ignored, relative to that of the parallelogram, in the limit $\epsilon \to 0$. The two wind profiles are

$$\overline{u}_i = \Lambda(z - z_i - \epsilon) \tag{3.1a}$$

$$\overline{u}_i = \Lambda(z - z_i), \tag{3.1b}$$

respectively, and their difference (lower minus upper) is $\epsilon\Lambda$. The change of momentum is therefore

$$\Delta M_i = \int_{z_m}^{z_p} \rho_0 \epsilon \Lambda \, dz + O(\epsilon^2)$$

$$= \rho_s \epsilon \Lambda H \left[\exp\left(-\frac{z_m}{H}\right) - \exp\left(-\frac{z_p}{H}\right) \right]_i + O(\epsilon^2), \tag{3.2}$$

where z_m and z_p are the lower and upper limits of the shear zone. Noting that

$$\rho_s B_i \Delta t = \Delta M_i = -\Delta z \rho_s \Lambda H[\cdots], \tag{3.3}$$

where B_i is the total wave momentum flux per unit mass absorbed by the shear zone (and $\epsilon = -\Delta z$), the rate of shear-zone descent is

$$\left(\frac{dz}{dt}\right)_i = -\frac{B_i}{\Lambda H[\cdots]} + \langle \overline{w}^* \rangle_i \tag{3.4}$$

due to wave absorption and upwelling, respectively; the quantity in brackets $[\cdots]$ was defined in (3.2). The upwelling term is calculated as a mass-weighted average over the depth of the shear zone, denoted by $\langle \cdots \rangle$. This average will be used in place of the mean momentum flux $\rho_0 \overline{uw}^*$ since the vertical velocity is divergent in the one-dimensional model. The vertical velocity inside the shear zone is simply

$$\overline{w}^* = a(z) \pm b(z)\Lambda, \tag{3.5}$$

using the regression (2.3), where the positive sign is chosen for westerly shear and vice versa (recall that $b < 0$). Vertical velocity has no effect outside the shear zones, where the vertical shear is zero. We are interested mainly in cases where shear zones descend (i.e., vertical advection does not overcome the effect of wave driving), although upward motion is possible and is sometimes observed in easterly shear zones before their demise.

Once the QBO envelope is specified in terms of limiting values of $\overline{u}$ and $\partial\overline{u}/\partial z$, together with vertical velocity $\overline{w}^*$, analytic solutions require knowledge of the momentum flux B_i imparted to each shear zone and the starting time for new shear zones aloft. Motivated by the discussion at the end of section 2, we assume that the incident flux is

$$B_{i,\text{in}} = f(\hat{u}_{i-1}), \tag{3.6}$$

where

$$\hat{u}_{i-1} = \pm\Lambda(z_{p,i-1} - z_{i-1}) \tag{3.7}$$

is the extremum of zonal wind below shear zone i (the choice of sign depending on the sign of the shear zone; the ordering is such that i, $i-1$, etc., refer to shear zones of the same sign). The net flux imparted to the shear zone is equal to the difference between incident and outgoing flux $B_{i,\text{out}}$, if any. In Fig. 7, for example, the overlying westerly shear zone (''A'' or ''B'') is accelerated by waves that survive to propagate above the tip of the lowest westerly jet. This flux is distributed across the entire shear zone, due to shear adjustment, even though the surviving spectrum encounters only the uppermost part of the shear zone. The *shape* of the source spectrum evidently affects the rate of shear-zone descent, given the same total flux and variation of $\hat{u}$; this problem is interesting to analyze in the simple model (see below).

The one-dimensional simulation discussed in section 2 indicates that a new westerly shear zone forms aloft as the faster Kelvin wave resumes its vertical propagation, coinciding approximately with the arrival of an easterly shear zone at the top of the westerly boundary

layer (specifically, when the *base* of the shear zone arrives at this point). Similarly, a new easterly shear zone forms when the Rossby-gravity wave resumes propagation, coinciding approximately with the arrival of a westerly shear zone at the top of the easterly boundary layer. This arrival occurs when zero-wind lines descend to a distance above the tropopause equal to approximately twice the depth of the respective boundary layers (noting that occlusion may increase this distance slightly). In the analytic model, a new shear zone is therefore assumed to form when the zonal wind begins to diminish at the top of the boundary layer. While relevant to the numerical model, this assumption is unrealistic since faster waves with phase speeds lying outside the QBO envelope constantly propagate upward and are responsible (in part) for the overlying semiannual oscillation (SAO). New QBO shear zones begin as SAO shear zones (Lindzen and Holton 1968; Dunkerton and Delisi 1997; D97); one can therefore imagine a more realistic upper boundary condition with imposed SAO (Holton and Lindzen 1972).

Descent of individual shear zones inside the QBO envelope is illustrated in Fig. 8, with $\overline{w}^* = 0$,

$$c_r = 25 \text{ m s}^{-1}, \tag{3.8a}$$

$$c_\ell = -35 \text{ m s}^{-1}, \tag{3.8b}$$

$$B_r(z_0) = 4 \times 10^{-3} \text{ m}^2 \text{ s}^{-2}, \tag{3.8c}$$

$$B_\ell(z_0) = -4 \times 10^{-3} \text{ m}^2 \text{ s}^{-2}, \tag{3.8d}$$

and two values of Λ. In the limit of infinite shear, the change of momentum in (3.2) reduces to

$$\Delta M_i = \rho_s \epsilon (c_r - c_\ell) \exp\left(-\frac{z_i}{H}\right) \tag{3.9}$$

and the descent time from infinity to the tropopause is

$$T = \frac{(c_r - c_\ell)H}{B(z_0)} \tag{3.10}$$

(Dunkerton 1981b) or 1215 days in this case ($H = 7$ km), as shown in Fig. 8a. Finite shear reduces the descent time, as shown in Fig. 8b, because the boundary layer now has finite depth, and in the boundary layer it is unnecessary to accelerate the flow all the way from one phase speed to the other. Elevation of the boundary layer top above the tropopause is therefore expected to reduce significantly the oscillation period, for reasons discussed above. The descent rate in Fig. 8b is asymmetric for finite Λ due to the asymmetry of phase speeds. The easterly shear zone has its ''center of mass'' at a higher altitude (i.e., lower density) than the westerly shear zone and is therefore easier to bring down initially, even though momentum fluxes are equal and opposite. On the other hand, the easterly shear zone must descend farther before encountering the top of the westerly boundary layer, which is shallower than the easterly boundary layer, compensating for the slightly faster initial descent. The compensation is exact, as it must be, since the amount of time to completely flip from one side of the envelope to the other is the same, going either way, for easterly and westerly forcings of equal amplitude.

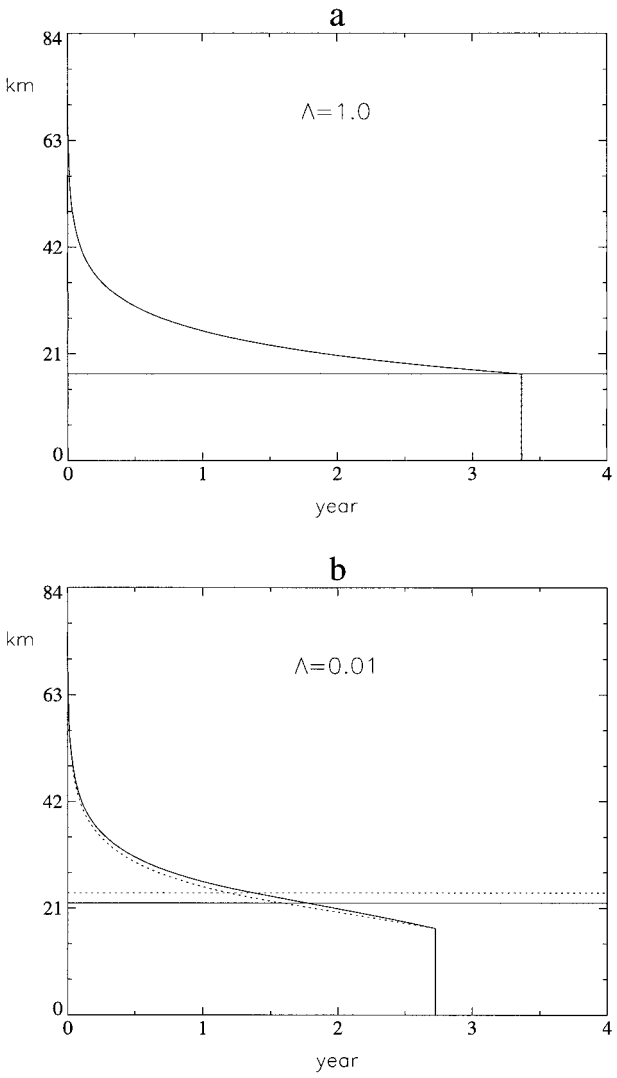

FIG. 8. Descent of individual westerly (solid) and easterly (dotted) shear zones in analytic solution for (a) $\Lambda \to \infty$ and (b) $\Lambda = 10$ m s^{-1} km^{-1}.

b. Two-wave case

The simplest problem is that of two discrete, conservative waves with phase speed c_r, c_ℓ and $\overline{w}^* = 0$. Each wave is responsible for its own shear zone and is cut off from further vertical propagation above the top of the shear zone where $\overline{u} = c_r$ (or c_ℓ). Vertical propagation to the top of the model resumes at full strength when the opposing shear zone arrives at the top of the

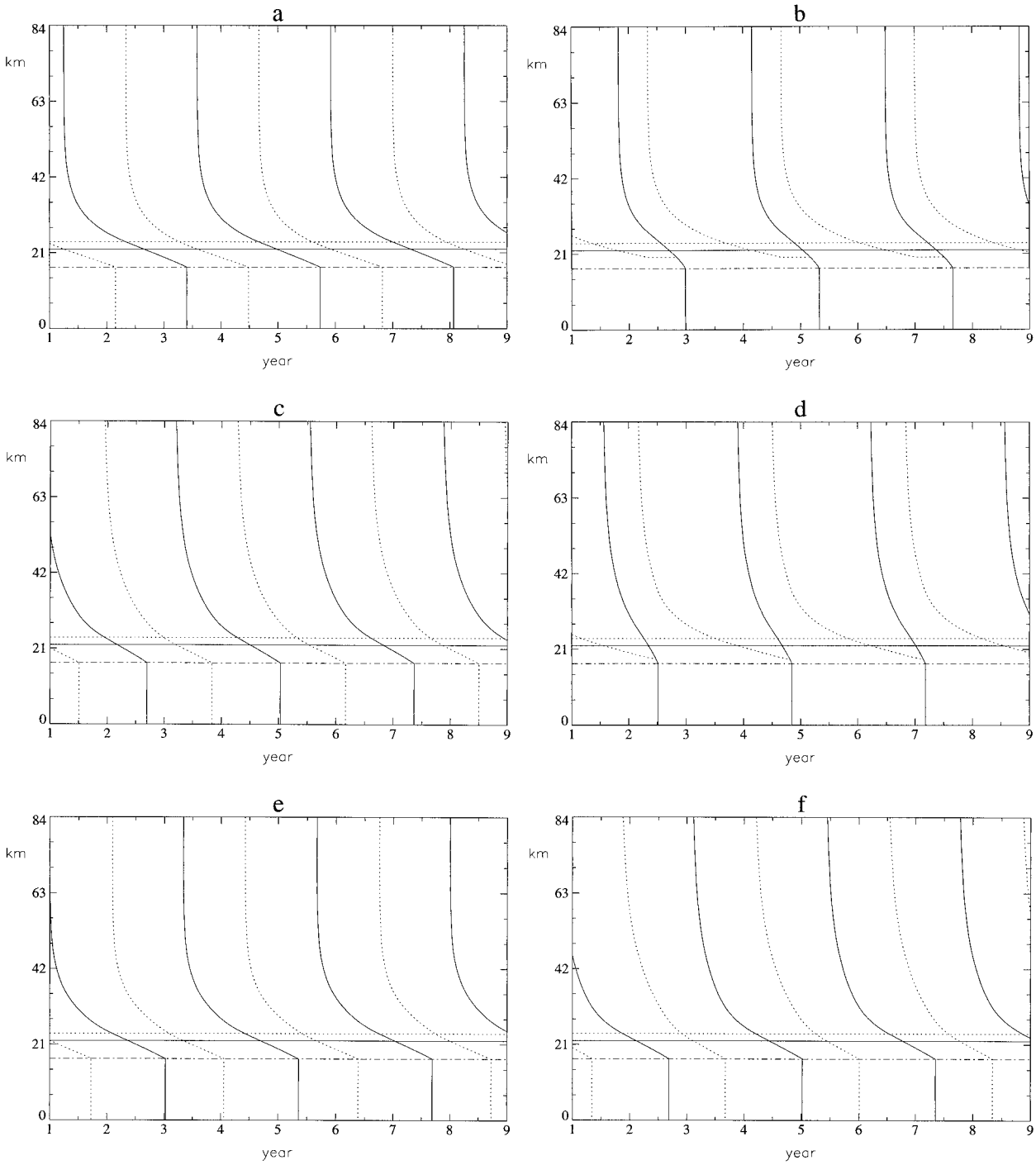

FIG. 9. Analytic solutions for various gravity wave spectra: (a), (b) Two-wave case with symmetric and asymmetric forcing, respectively; (c), (d) white spectrum with symmetric and asymmetric forcing, respectively; (e) combination of two waves and red spectrum; and (f) red spectrum only. Forcing amplitudes were adjusted to produce a QBO with period 840 days in each case, and $\overline{w} = 0$.

boundary layer. This (extreme) situation is illustrated in Fig. 9a for equal and opposite forcings but with asymmetric phase speeds as in (3.8a) and (3.8b). With $\overline{w}^* = 0$, the oscillation period is inversely proportional to forcing amplitude. The forcing has therefore been adjusted to produce a period of 840 days, in this example and others to follow, in order to highlight differences in vertical structure. Horizontal lines in Fig. 9a indicate a position above the tropopause equal to twice the depth of nominal boundary layers without occlusion:

$$z_0 + 2h_r = z_0 + 2c_r/\Lambda \quad (3.11a)$$

$$z_0 + 2h_\ell = z_0 - 2c_\ell/\Lambda. \quad (3.11b)$$

Note that a new easterly shear zone begins when the zero-wind line in the westerly shear zone arrives at $z_0 + 2h_\ell$, and vice versa (coinciding with the arrival of the base of the westerly shear zone at the top of the easterly boundary layer $z_0 + h_\ell$, and vice versa). The required forcing is 5.075×10^{-3} m^2 s^{-2} for each wave (in absolute value).

With asymmetric forcing it is easy to achieve occlusion in the two-wave model. An example with 2:1 ratio of westerly to easterly forcing is shown in Fig. 9b. The required forcing is 6.956×10^{-3} m^2 s^{-2} for the westerly wave and half of this value for the easterly wave. Note that the lower easterly shear zone stalls when the base of the overlying westerly shear zone intersects the top of the easterly shear zone. At this moment, the zero-wind line in the westerly shear zone is a little higher than $z_0 + 2h_\ell$. When a new easterly shear zone begins, the older shear zone is no longer able to absorb easterly momentum flux. Descent of the westerly shear zone accelerates after this time (relative to that of Fig. 8a) because it is riding down the back of the (stalled) easterly shear zone at a higher altitude than before, so that less momentum is required to switch to westerlies. The vertical structure is markedly asymmetric with longer duration of westerlies at low levels and vice versa.

c. White spectrum

If the momentum flux in the source spectrum is spread evenly between $c = 0$ and c_r (or c_ℓ)—a more realistic situation—the effect is to divide the flux between old and new shear zones once a new shear zone is formed. Descent of the new shear zone is slower than in the two-wave problem, while descent of the old shear zone is more persistent, making occlusion more difficult to achieve. With symmetric forcing (but asymmetric c_r, c_ℓ) the result is shown in Fig. 9c. The required forcing amplitude, 7.251×10^{-3} m^2 s^{-2}, is larger than before. The white spectrum is less efficient because some of the momentum flux is wasted in old shear zones, slowing the descent of new shear zones. With a white spectrum, greater asymmetry is required for occlusion. An example with 6:1 ratio of westerly to easterly forcing is shown in Fig. 9d. The required forcing is 24.35×10^{-3} m^2 s^{-2} for the westerly wave and one-sixth of this value for the easterly wave. Unlike the two-wave case, the old easterly shear zone continues to descend after the new easterly shear zone begins. The vertical structure is asymmetric once again.

d. Red spectrum

The least efficient forcing is a red spectrum of momentum flux, as in (2.8). Using this spectrum in combination with a pair of discrete waves illustrates a modest sensitivity of oscillation period to the spectral form. For the sake of this example, assume that the spectrum is truncated at c_r, c_ℓ and that these values again define the QBO envelope above the boundary layer. When the flux is divided about equally between the discrete and continuous spectrum, the required forcing is 6.807×10^{-3} m^2 s^{-2} for the discrete waves, while the value of $B_{\rm GW}(z_0)$ is twice as large, as shown in Fig. 9e. But when the continuous spectrum contains all of the momentum flux, the required value of $B_{\rm GW}(z_0)$ is 18.82×10^{-3} m^2 s^{-2}, as shown in Fig. 9f.

e. Realistic case

The combined spectrum in the preceding example is similar to the situation described in section 2 except that in the numerical model, discrete equatorial waves continue to experience damping in the boundary layer after a new shear zone is formed aloft, and the vertical velocity is nonzero. In order to model the absorption of discrete waves, the data in Fig. 6 were approximated by a smooth function for each wave, using for $\hat{u}_{i-1}$ in (3.7) the maximum (or minimum) wind in the boundary layer. Equatorial wave forcings were assigned as in section 2. Values of c_r, c_ℓ in (3.8a) and (3.8b) were assumed for maximum QBO winds, as suggested by Fig. 4, rather than the equatorial wave phase speeds. The vertical velocity was incorporated using (3.4) and (3.5). Two examples are shown in Figs. 10a,b. The gravity wave forcing was varied slightly to yield a QBO period of 974 and 727 days, using values of $B_{\rm GW}(z_0) = 26$ and 30×10^{-3} m^2 s^{-2}, respectively. A modest increase of forcing is consistent with results presented in section 4 since the QBO period can be reduced by increasing the diffusion of momentum. The analytic solution is inviscid (apart from shear adjustment) and requires a slightly larger gravity wave flux compared to the numerical solution with Pr = 1. In other respects, the analytic solution captures the behavior of the simulated QBO with a shallow occlusion, relatively fast initial descent of easterly shear zones followed by much slower descent, and asymmetric vertical structure. The occlusion deepens as the gravity wave flux is reduced, while the oscillation period increases and vice versa.

4. More numerical results

Values of constituent diffusivity derived from the tape recorder effect are small compared to the momentum diffusivity used in previous QBO modeling. Diffusion plays a minor role in the numerical model, rounding off the westerly and easterly jets at the top of the boundary layer. Experiments performed with other values of Pr reveal that the QBO period is rather insensitive to Pr from 0.1 to 1, so that the model run highlighted in section 2e approximates the (otherwise) inviscid limit. Variation of QBO period as a function of $B_{\rm GW}(z_0)$ is illustrated in Figs. 11a,b with and without α, the in-

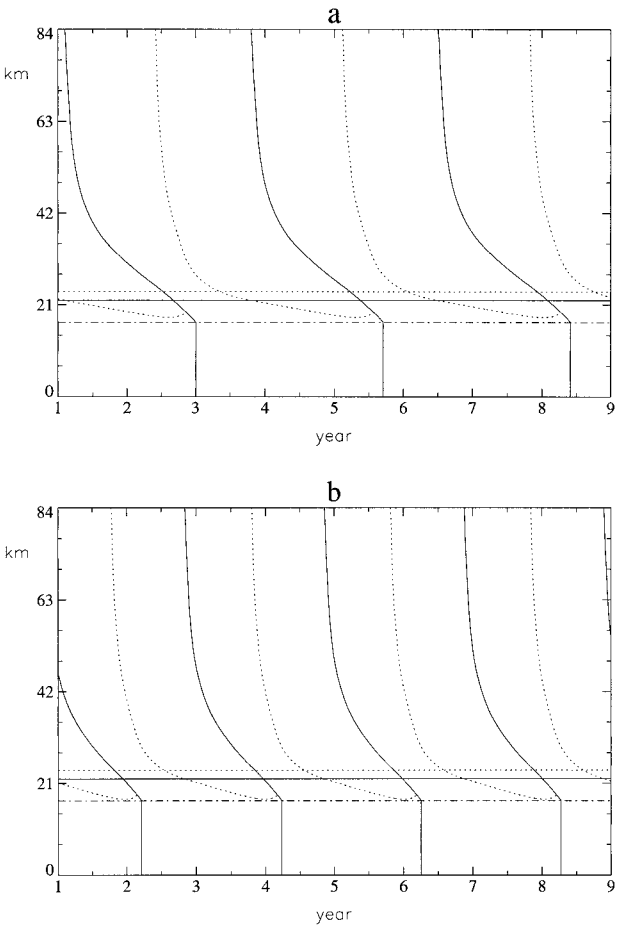

FIG. 10. Analytic solutions in realistic case with vertical velocity and approximate equatorial wave damping $P(z)$ derived from Fig. 6. (b) The gravity wave flux was increased slightly.

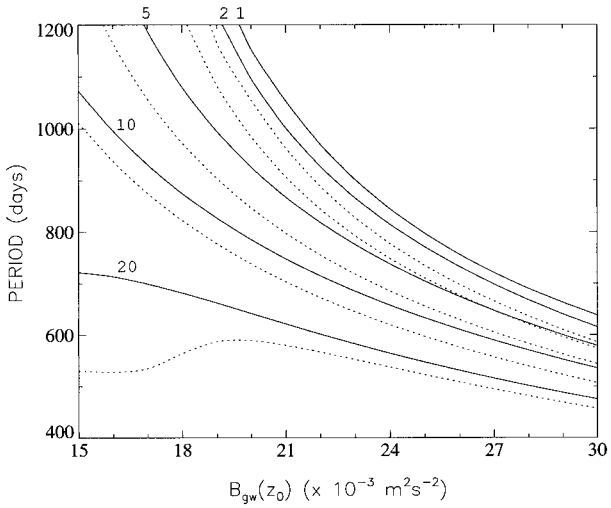

FIG. 11. Variation of QBO period as a function of $B_{GW}(z_0)$ for various Pr, with frictional damping α (dotted) and without frictional damping (solid).

mixing rate derived from the tape recorder effect. Oscillation period diminishes with increased forcing or Pr, as expected. Friction reduces the period slightly, noting that the change of $\overline{u}$ from one phase to the other is reduced below the shear zone (Fig. 4) so that for the same flux of momentum, shear zones should descend more rapidly. Similar variation of QBO period with forcing amplitude is observed in the analytic solution (corresponding to the ''realistic'' case described in section 3e) but slightly larger fluxes are required, especially at longer periods.

The vertical structure of numerical QBOs for various Pr is illustrated in Fig. 12. In each case, the gravity wave flux was adjusted to produce an oscillation with period ~840 days. The structure is fairly realistic for Pr in the range 2–5, while it is becoming unrealistic for Pr = 10. In this case, the effect of diffusion above the tropopause is clearly seen. No solution with 840-day period exists for Pr = 20; at this value of Pr, the structure is severely affected by diffusion, making such a large Prandtl number unlikely outside of QBO shear zones. One desirable feature of solutions with Pr > 1 is a more rounded amplitude profile above the tropopause, instead of a discontinuous slope as in the analytic solution and nearly inviscid numerical solutions.

Similar experiments were performed with $\Lambda = 15$ m s^{-1} km^{-1} and the results (not shown) are qualitatively similar to those discussed above, except that larger values of gravity wave flux are required to achieve comparable QBO period.

5. Conclusions

Observations of ascending water vapor anomalies in the tropical lower stratosphere—the so-called tape recorder effect—have been used to infer profiles of vertical mean motion, vertical constituent diffusivity, and lateral in-mixing rate in this region (Mote et al. 1998). The magnitude of vertical wave flux required to drive the quasi-biennial oscillation (QBO) in the presence of mean upwelling, along with other related aspects of QBO dynamics, was examined in light of the tape recorder results using a simple one-dimensional model. As found in a previous study (D97) it is necessary that wave fluxes significantly exceed the ''classic'' values associated with long-period Kelvin and Rossby-gravity waves; the extra fluxes are presumably associated with a continuous spectrum of short-period gravity and inertia–gravity waves. Larger wave fluxes, when used in connection with traditional wave-transport parameterizations developed for the QBO, require a larger vertical diffusivity of momentum in order to prevent the formation of unrealistically strong vertical wind shear. The profile of constituent diffusivity derived from the tape recorder effect, however, is everywhere much smaller than the momentum diffusivity assumed in previous QBO modeling studies—so much smaller, in fact, as to be almost irrelevant to the dynamics. Lateral in-mixing,

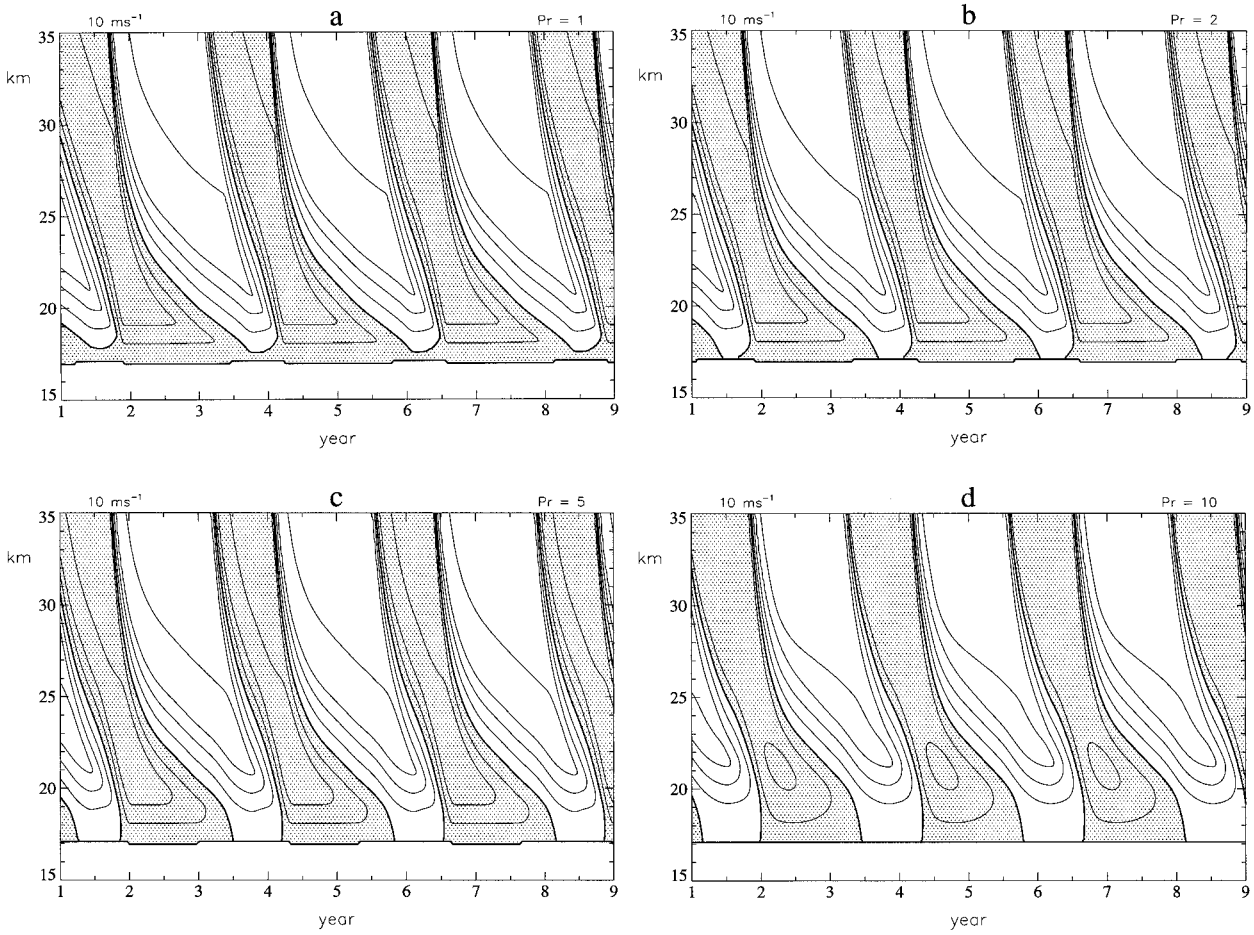

FIG. 12. Mean zonal wind in the numerical model: (a) Pr = 1, (b) Pr = 2, (c) Pr = 5, and (d) Pr = 10. The gravity wave forcing $B_{GW}(z_0)$ was adjusted to produce a QBO with period 840 days in each case. Contour interval 10 m s^{-1}, and westerlies are shaded.

parameterized as Rayleigh friction, has only a small effect on the numerical solution and does not alleviate the problem. This finding implies either that the wave-transport parameterization is inappropriate for the QBO, or that the effective turbulent Prandtl number is significantly greater than unity. It is unlikely that the true momentum diffusivity is temporally constant; shear instabilities are probably enhanced in QBO shear zones, where mixing is most required, according to the model.

Realistic shear is obtained in the model using a momentum-conserving shear adjustment scheme representing the effect of unresolved shear instabilities and other processes not included in the wave-transport parameterization. This device, together with a QBO amplitude profile based on the equatorial wave phase speeds, motivates an (otherwise inviscid) analytic QBO solution in the underdamped, quasi-compressible case. The simple analytic solutions replicate most aspects of the numerical solution, display a similar dependence on wave flux at the lower boundary and provide reasonably accurate estimates of QBO period in the inviscid limit. When the turbulent Prandtl number is increased above unity, the QBO period decreases, so that a slightly smaller wave flux is adequate, and the vertical structure is more realistic near the tropopause. The analytic solution is inviscid except for shear adjustment, and viscous damping of the jet maximum is neglected. This damping might be important in situations where the source spectrum has a momentum flux peak near the maximum jet speed, making the evolution sensitive to diffusion of the extrema. With smooth spectra the oscillation should not be sensitive to weak diffusion and resulting small variations of jet strength.

The analytic solution is valuable not only for estimating QBO behavior but also in focusing the discussion of QBO dynamics on three issues of importance, namely, the vertical amplitude profile of the QBO, the strength of mean vertical shear, and shape of the momentum flux spectrum.

a. Oscillation amplitude

Prediction of QBO amplitude is simplified if two discrete equatorial waves determine the maximum range

of mean flow speeds (Holton and Lindzen 1972). The spectrum of Kelvin and Rossby-gravity waves (and of other equatorial waves) is actually broad, yet the amplitude of the observed QBO seems remarkably constant in time and height (above the boundary layer and below the SAO region). As noted by Li et al. (1997), there is a ''spectral window'' of phase speeds able to affect the stratosphere. Slower waves fail to reach the stratosphere, while faster waves propagate without attenuation or become evanescent. The spectral window is too broad, however, to explain precisely the amplitude of the QBO. Our simple model follows Holton and Lindzen (1972), giving a realistic amplitude; the addition of continuous gravity wave spectrum following Lindzen and Holton (1968) leaves the maximum amplitude unaffected. The analytic solution therefore applies and is reasonably accurate. In the general case, the QBO amplitude is not known a priori, and may depend on the forcing amplitude. An interesting example is related by Saravanan (1990) in which a spectral ''tail'' was added to a white spectrum of damped waves. In this case, the QBO amplitude is approximately proportional to forcing amplitude. For the analytic solution to be useful in general, it will be necessary to predict the amplitude envelope theoretically rather than numerically.

b. Shear-zone strength and boundary layer depth

Factors that determine the strength of QBO shear zones and the depth of QBO boundary layer above the tropopause are not well understood. It is clear from the analytic and numerical solutions that the period of the QBO is sensitive to the depth of the boundary layer.[1] In a quasi-compressible atmosphere, the amount of mass involved in the QBO is determined by the altitude at which the oscillation attains maximum amplitude; each density-scale height corresponds to a factor of *e*. The generation of new shear zones aloft depends on the time required for existing shear zones to descend to the top of the boundary layer. A taller boundary layer shortens the distance to descend and thereby speeds up the oscillation. The QBO period is also sensitive to in situ shear strength because the temperature and induced circulation are proportional to $\partial\overline{u}/\partial z$. If the easterly shear is too strong, its descent will be slowed excessively, or completely stalled.

c. Momentum flux spectrum

The shape of the momentum flux spectrum as a function of phase speed determines where momentum deposition occurs in the QBO, whether in an old shear zone near the tropopause or a new shear zone aloft. An *efficient* spectrum concentrates the momentum flux near the extrema of the QBO so that this flux is available to new shear zones as early as possible. For this reason, the observed large-scale equatorial waves with phase speed close to the maximum QBO wind speeds are probably the most important part of the spectrum. These waves not only contain a significant fraction of the total momentum flux but are free to resume their vertical propagation to upper levels when QBO regimes begin to decay at lower levels. Waves in the gravity wave spectrum with slower phase speed gradually resume their propagation as boundary layer winds continue to decay. Gravity waves, nonetheless, are essential to the QBO in order to overcome the effect of Brewer–Dobson upwelling (D97). Evolution of the QBO is therefore thought to occur in two stages: the large-scale equatorial waves establish a new QBO shear zone aloft (or extend the descent of an existing SAO shear zone), while gravity waves assume greater importance as the shear zone descends.

Observational evidence supporting the role of a gravity wave spectrum is mostly circumstantial (D97). Further studies concentrating on this part of the spectrum (including inertia–gravity waves of period ~1–3 days) are necessary. Detailed analysis of the wave spectrum and the dynamics of QBO shear zones should lead to a better understanding of the oscillation.

Acknowledgments. This research was supported by National Science Foundation Grant ATM-9500613 and National Aeronautics and Space Administration Contract NAS1-96071.

[1] Spontaneous QBOs in general circulation models therefore should be evaluated in terms of the altitude of the simulated oscillation and boundary layer depth. For the same vertical flux of momentum, a QBO confined to higher altitudes is likely to have a shorter period, and may be easier to achieve, than a QBO with realistic vertical structure above the tropopause.

REFERENCES

Andrews, D. G., and M. E. McIntyre, 1976: Planetary waves in horizontal and vertical shear: The generalized Eliassen–Palm relation and the mean zonal acceleration. *J. Atmos. Sci.,* **33,** 2031–2048.

Bergman, J. W., and M. L. Salby, 1994: Equatorial wave activity derived from fluctuations in observed convection. *J. Atmos. Sci.,* **51,** 3791–3806.

Broutman, D., C. Macaskill, M. E. McIntyre, and J. W. Rottman, 1997: On Doppler-spreading models of internal waves. *Geophys. Res. Lett.,* **24,** 2813–2816.

Chen, P., 1995: Isentropic cross-tropopause mass exchange in the extratropics. *J. Geophys. Res.,* **100,** 16 661–16 673.

Coy, L., and D. C. Fritts, 1988: Gravity wave heat fluxes: A Lagrangian approach. *J. Atmos. Sci.,* **45,** 1770–1780.

Delisi, D. P., and T. J. Dunkerton, 1989: Laboratory observations of gravity wave critical-layer flows. *Pure Appl. Geophys.,* **130,** 445–461.

Dunkerton, T. J., 1981a: Wave transience in a compressible atmosphere. Part I: Transient internal wave, mean-flow interaction. *J. Atmos. Sci.,* **38,** 281–297.

——, 1981b: Wave transience in a compressible atmosphere. Part II: Transient equatorial waves in the quasi-biennial oscillation. *J. Atmos. Sci.,* **38,** 298–307.

——, 1985: A two-dimensional model of the quasi-biennial oscillation. *J. Atmos. Sci.,* **42,** 1151–1160.

——, 1990: Annual variation of deseasonalized mean flow acceleration in the equatorial lower stratosphere. *J. Meteor. Soc. Japan,* **68,** 499–508.
——, 1991: Nonlinear propagation of zonal winds in an atmosphere with Newtonian cooling and equatorial wavedriving. *J. Atmos. Sci.,* **48,** 236–263.
——, 1995: Evidence of meridional motion in the summer lower stratosphere adjacent to monsoon regions. *J. Geophys. Res.,* **100,** 16 675–16 688.
——, 1997: The role of gravity waves in the quasi-biennial oscillation. *J. Geophys. Res.,* **102,** 26 053–26 076.
——, and D. C. Fritts, 1984: Transient gravity wave–critical layer interaction. Part I: Convective adjustment and the mean zonal acceleration. *J. Atmos. Sci.,* **41,** 992–1007.
——, and D. P. Delisi, 1985: Climatology of the equatorial lower stratosphere. *J. Atmos. Sci.,* **42,** 376–396.
——, and ——, 1997: Interaction of the quasi-biennial oscillation and stratopause semiannual oscillation. *J. Geophys. Res.,* **102,** 26 107–26 116.
Fels, S. B., 1982: A parameterization of scale-dependent radiative damping rates in the middle atmosphere. *J. Atmos. Sci.,* **39,** 1141–1152.
Fritts, D. C., and T. J. Dunkerton, 1985: Fluxes of heat and constituents due to convectively unstable gravity waves. *J. Atmos. Sci.,* **42,** 549–556.
Hall, T. M., and D. Waugh, 1997: Tracer transport in the tropical stratosphere due to vertical diffusion and horizontal mixing. *Geophys. Res. Lett.,* **24,** 1383–1386.
Hamilton, K., 1984: Mean wind evolution in the tropical lower stratosphere. *J. Atmos. Sci.,* **41,** 2113–2125.
Hazel, P., 1972: Numerical studies of the stability of inviscid stratified shear flows. *J. Fluid Mech.,* **51,** 39–61.
Hitchman, M. H., M. McKay, and C. R. Trepte, 1994: A climatology of stratospheric aerosol. *J. Geophys. Res.,* **99,** 20 689–20 700.
Holton, J. R., and R. S. Lindzen, 1972: An updated theory for the quasi-biennial cycle of the tropical stratosphere. *J. Atmos. Sci.,* **29,** 1076–1080.
Li, X., P. L. Read, and D. G. Andrews, 1997: Mode selection, wave breaking and parametric sensitivity in the quasi-biennial oscillation. *Quart. J. Roy. Meteor. Soc.,* **123,** 2041–2068.
Lindzen, R. S., and J. R. Holton, 1968: A theory of the quasi-biennial oscillation. *J. Atmos. Sci.,* **25,** 1095–1107.
Maruyama, T., 1994: Upward transport of westerly momentum due to disturbances of the equatorial lower stratosphere in the period range of about 2 days—A Singapore data analysis for 1983–1993. *J. Meteor. Soc. Japan,* **72,** 423–432.
Mote, P. W., and Coauthors, 1996: An atmospheric tape recorder: The imprint of tropical tropopause temperatures on stratospheric water vapor. *J. Geophys. Res.,* **101,** 3989–4006.
——, T. J. Dunkerton, M. E. McIntyre, E. A. Ray, P. H. Haynes, and J. M. Russell III, 1998: Vertical velocity, vertical diffusion, and dilution by midlatitude air in the tropical lower stratosphere. *J. Geophys. Res.,* **103,** 8651–8666.
Naujokat, B., 1986: An update of the observed quasi-biennial oscillation of the stratospheric winds over the tropics. *J. Atmos. Sci.,* **43,** 1873–1877.
Ortland, D. A., 1997: Rossby wave propagation into the tropical stratosphere observed by the High Resolution Doppler Imager. *Geophys. Res. Lett.,* **24,** 1999–2002.
O'Sullivan, D. J., 1997: Interaction of extratropical Rossby waves with westerly quasi-biennial oscillation winds. *J. Geophys. Res.,* **102,** 19 461–19 449.
——, and T. J. Dunkerton, 1997: The influence of the quasi-biennial oscillation on global constituent distributions. *J. Geophys. Res.,* **102,** 21 731–21 743.
Plumb, R. A., 1977: The interaction of two internal waves with the mean flow: Implications for the theory of the quasi-biennial oscillation. *J. Atmos. Sci.,* **34,** 1847–1858.
——, and A. D. McEwan, 1978: The instability of a forced standing wave in a viscous stratified fluid: A laboratory analog of the quasi-biennial oscillation. *J. Atmos. Sci.,* **35,** 1827–1839.
——, and R. C. Bell, 1982: A model of the quasi-biennial oscillation on an equatorial beta-plane. *Quart. J. Roy. Meteor. Soc.,* **108,** 335–352.
Rosenlof, K. H., 1995: Seasonal cycle of the residual mean meridional circulation in the stratosphere. *J. Geophys. Res.,* **100,** 5173–5191.
Saravanan, R., 1990: A multiwave model of the quasi-biennial oscillation. *J. Atmos. Sci.,* **47,** 2465–2474.
Sato, K., and T. J. Dunkerton, 1997: Estimates of momentum flux associated with equatorial Kelvin and gravity waves. *J. Geophys. Res.,* **102,** 26 247–26 261.
Schoeberl, M. R., A. E. Roche, J. M. Russell III, D. Ortland, P. B. Hays, and J. W. Waters, 1997: An estimation of the dynamical isolation of the tropical lower stratosphere using UARS wind and trace gas observations of the quasi-biennial oscillation. *Geophys. Res. Lett.,* **24,** 53–56.
Stone, P. H., 1966: On non-geostrophic baroclinic stability. *J. Atmos. Sci.,* **23,** 390–400.
Trepte, C. R., and M. H. Hitchman, 1992: The stratospheric tropical circulation deduced from aerosol satellite data. *Nature,* **355,** 626–628.
——, R. E. Veiga, and M. P. McCormick, 1993: The poleward dispersal of Mount Pinatubo volcanic aerosol. *J. Geophys. Res.,* **98,** 18 563–18 573.